

# Convex Optimization-based Control Design for Parallel Grid-Connected Inverters

Christoph Kammer<sup>1</sup>, Salvatore D'Arco<sup>2</sup>, Atsede Gualu Endegnanew<sup>2</sup>, Alireza Karimi<sup>1</sup>

**Abstract**—This paper presents a novel frequency-domain approach towards the control design for parallel grid-connected voltage source inverters (VSIs) with LCL output filters. The proposed method allows to design the controllers of multiple VSIs in a single step, and inherently attenuates the resonances introduced by the output filters and coupling effects while guaranteeing stability. Performance specifications such as desired closed-loop bandwidth, decoupling or robustness towards multi-model uncertainty can be specified through frequency-domain constraints. Furthermore, controllers can be designed in a plug-and-play fashion. The designed controllers are equivalent in structure to multivariable PI controllers with filters. As the control design is based on the frequency response of the system, the algorithm is independent of the model order, which allows the use of large and high-order models. The performance of the method is demonstrated on a relevant example of a low-voltage distribution grid with 5 VSIs, and the results are validated both in numerical simulation using MATLAB/Simulink as well as in power-hardware-in-the-loop experiments.

**Index Terms**—Resonance, H-infinity control, Power system transients, Robustness, Current control

## I. INTRODUCTION

In recent years, the growth of distributed generation, distributed storage and drive loads has led to a significant increase in penetration of power electronics in distribution grids. These devices are commonly interfaced to the grid through voltage source inverters (VSIs) with passive output filters. A desirable filter structure for grid connected converters is the LCL filter, which exhibits many advantageous features. However, the parallel operation of VSIs with LCL filters introduces new resonance frequencies and dynamic coupling effects into the grid. More power electronics converters may also be added at subsequent stages and their controllers should be designed for a "plug-and-play" installation without negatively affecting the grid and the operation of the already existing converters. Moreover, distribution grids with relatively large shares of distributed generation are more susceptible to overvoltages, which are commonly prevented by installing additional Line Voltage Regulators (LVRs). These conditions translate into

The work presented in this paper was supported by the Swiss Federal Commission for Innovation and Technology within the SCCER-FURIES.

This paper has been achieved using the ERIGrid Research Infrastructure and is part of a project that has received funding from the European Unions Horizon 2020 Research and Innovation Programme under the Grant Agreement No. 654113.

C. Kammer and A. Karimi are with the Laboratoire d'Automatique, École Polytechnique Fédérale de Lausanne, 1015 Lausanne, Switzerland. S. D'Arco and A. Endegnanew are with the SINTEF Energy Research, 7465 Trondheim, Norway.

Corresponding author: alireza.karimi@epfl.ch, Tel. +41 21 69 35925

challenges for stability analysis and control design [1], [2], [3], [4], [5] since the VSI controllers have to be robust towards changes in the grid layout, and have to guarantee performance for highly uncertain and time-varying line impedances.

Several active damping methods have been proposed in the literature for mitigating the effect of LCL output filter resonances, and a comprehensive review of the state-of-the-art is given in [6]. A common approach is to introduce active filter elements to the feedback loop and tune the parameters based on the model of a single-inverter infinite bus system. However, using a single-inverter model neglects all coupling dynamics in the grid and gives no guarantee for stability or performance in a system with multiple VSIs. Thus, approaches specifically aimed towards control design and stability analysis in grids with multiple VSIs have been proposed. For example, the tuning of current controllers for an arbitrary number of parallel inverters for PhotoVoltaic (PV) generation is presented in [7], [8] assuming identical VSIs. In [9], [10], [11] a state-space model of the complete system is constructed, and the resonance modes are classified based on modal participation factors. Another approach is breaking the system into interconnected component models that are easier to handle than the full system and then apply impedance-based transfer function models to tune filters in the frequency domain [5], [12]. In [13] a multivariable transfer function model for grids with multiple VSIs is developed, and it is shown that the model can be used for stability analysis through Nyquist diagrams. The modeling approach is further used in [14], [15] to derive design rules for proportional controllers based on root locus curves. A main issue of these methods is that the design is based on iterative procedures and does not scale well for more complex controller structures and larger systems. Furthermore, it is difficult to achieve explicit robustness and performance specifications, especially for uncertain systems.

Optimization-based robust control design methods with  $H_\infty$  and  $H_2$  performance criteria can guarantee robust stability and performance, and allow the design of higher-order controllers that would be very challenging to tune using iterative procedures. These optimization-based methods have been applied for tuning of controllers in grid connected VSIs, but, to the authors best knowledge, the references available in the literature are limited to single-inverter systems, while configurations with multiple inverters have not yet been considered. In [16], [17], [18] full-order  $H_\infty$  methods are used to design current controllers for single VSIs by solving the mixed sensitivity problem. Similarly, in [19] a full-order  $\mu$ -synthesis method is employed to guarantee robustness against parametric model uncertainty. A significant drawback of full-order methods is

that no controller structure can be imposed, meaning they can only be used to design centralized controllers. However, for parallel inverters a decentralized structure is required in practice, which means that full-order methods are not suitable. To overcome this limitation, fixed-structure methods are preferred since the order and structure of the controller can be chosen as part of the design parameters. In [20], [21], [22] methods based on Lyapunov functions are proposed, but they do not scale well with the number of states of the plant, making it difficult to solve cases with multiple inverters efficiently. In [23] a non-convex fixed-structure method is used to compute gain-scheduled PI controllers, but the scope is again limited to a single grid-connected VSI.

The majority of robust control methods require a parametric state space model of the plant for the design, and result in a continuous-time state-space controller. However, a parametric state space formulation suffers from the inherent disadvantage that accurate plant models can be difficult to obtain. Furthermore, time delays in the controller or plant are difficult to consider in a state-space framework. These issues can be avoided by applying frequency response methods, which require only the frequency response of the plant for the design. This makes the design independent of the order and number of states of the plant, and enables a more data driven approach. Furthermore, discrete-time controllers can be designed directly without a controller discretization step and time delays can be considered exactly. In [24], [25] a method is demonstrated that allows to compute a PI current controller for a single grid connected VSI purely based on measurement data. The same approach is also used in [26] to tune a higher order current controller for a single VSI with an LCL output filter. However, the method applied in these papers only allows for linearly parametrized controllers, and generally yields very conservative results for coupled multivariable systems.

This paper presents a novel frequency response method for robust control design of parallel grid-connected inverters, which is based on the theoretical formulation for multivariable systems recently introduced in [27]. Since the method is tailored for multivariable systems, this paper effectively extends the applicability of the control principles introduced in [24], [25], [26] and their benefits to grid configurations with multiple converters. This approach allows the tuning of the fixed structure controllers of an arbitrary number of VSIs in a single step while guaranteeing stability, performance and robustness towards variation of the grid configuration. The method requires as inputs the frequency response data of the system to be controlled, the parametric structure of the controllers and a set of frequency domain performance specifications and constraints. These inputs are then translated into a convex optimization problem whose solution defines the controller parameters. The main advantages offered compared to the more conventional existing methods can be summarized as:

- The controller synthesis requires only the frequency response of the plant, which offers more flexibility for obtaining the model compared to methods based on a state space formulation as explained above. This includes also the possibility of a purely data-driven specification of the

plant (e.g. from an experimentally measured frequency response).

- The method allows to combine  $H_2$ ,  $H_\infty$  and loop-shaping performance objectives, resulting in a very flexible and intuitive problem formulation.
- Robustness versus modelling uncertainties and multi-model uncertainty (e.g. changes in the grid topology) is straightforward to consider.
- The method is very scalable and allows the use of very detailed and high-order models without increasing the complexity of the design process.
- Discrete-time controllers are designed directly based on a continuous-time plant model. No controller discretization step is necessary, and time delays can be considered exactly.
- Controllers are fully parametrized, which allows to achieve better performance with a smaller number of tuning parameters. This parametrization encompasses many common structures, such as the multivariable PI controller with resonance filters.

The design method is first presented in Section II, and then illustrated with a comprehensive example consisting in the tuning of the current controllers of 4 VSIs in a typical low-voltage distribution grid. In order to demonstrate robustness, the controllers are tuned to fulfill the design specifications with or without the presence of an LVR. Furthermore, it is presented how a current controller can be designed in a pure plug-and-play fashion by showing that a new VSI can be added while still guaranteeing stability and performance. The performance of the controllers is validated against the desired specifications in numerical simulations in the Matlab/Simulink environment and on an experimental setup. The experiments have been conducted according to a power-hardware-in-the-loop (PHIL) approach, where three 60 kW converter units have been tested together with an electrical grid and two more converter units simulated in real time.

## II. FREQUENCY-DOMAIN CONTROL DESIGN METHOD BASED ON CONVEX OPTIMIZATION

This section presents the application of a novel control design method that can be used to tune the controllers of any number of VSIs directly in discrete-time, while guaranteeing stability and performance. The method is used to compute fixed-structure, robust controllers, which are very common in industrial applications (a classical example would be a multiple-input multiple-output PID controller with filters). This section aims to give a general overview of how typical time-domain performance specifications can be formulated in the frequency domain. Also, common controller structures are discussed. A full theoretical exposition of the method can be found in [27].

The parameters required for the design can be grouped into three categories, which are discussed in the following subsections: the frequency response data of the system, the desired controller structure, and the frequency-domain design parameters that describe the desired performance. The main steps of the design process are shown in Fig. 1, and will be detailed in the following sections.

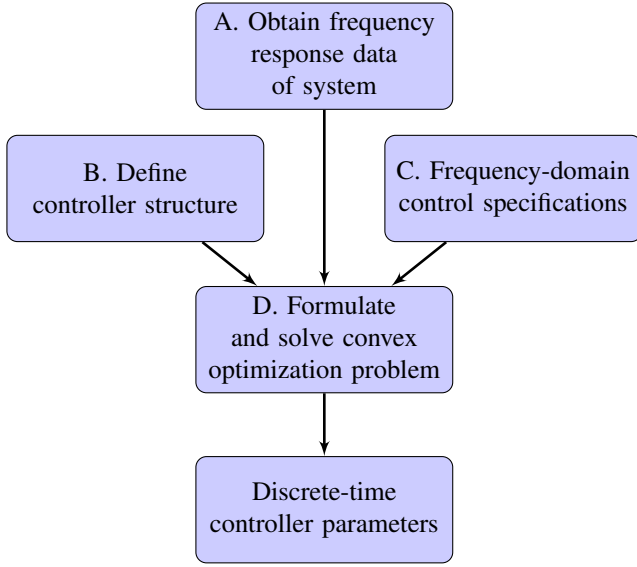


Fig. 1. The main steps of the control design algorithm.

### A. Specification of System Frequency Response

Robust control design methods generally require a state space model of the system to be controlled. However, the control design method presented in this paper requires only the frequency response  $G(j\omega) \in \mathbb{C}^{n \times m}$  of the plant, where  $m$  is the number of inputs and  $n$  is the number of outputs. The frequency response of a plant can be derived either from a parametric model or from time-domain measurements. If a parametric model is used, the frequency response is obtained by evaluating:

$$G(j\omega) = G(s = j\omega), \quad \omega \in \Omega = \{\omega \mid -\infty < \omega < \infty\} \quad (1)$$

Alternatively,  $G(j\omega)$  can be identified from time-domain measurements from  $m$  sets of input/output sampled data by applying the Fourier analysis as:

$$G(j\omega) = \left[ \sum_{k=0}^{N-1} y(k) e^{-j\omega T_s k} \right] \left[ \sum_{k=0}^{N-1} u(k) e^{-j\omega T_s k} \right]^{-1} \quad (2)$$

$$\omega \in \Omega = \left\{ \omega \mid -\frac{\pi}{T_s} \leq \omega \leq \frac{\pi}{T_s} \right\}$$

Thus, the presented design method offers a degree of flexibility in specifying the system and allows for a purely data-driven approach, where no parametric white-box model is necessary. Moreover, the control design is practically independent of the number of states of the model, allowing for more accurate and higher order representations of the system without any drawback.

### B. Definition of Controller Structure

The controller structure is defined as  $K(z) = X(z)Y(z)^{-1}$ , where  $X(z)$  and  $Y(z)$  are transfer function matrices of order  $p$ :

$$X(z) = (X_p z^p + \dots + X_1 z + X_0) \circ F_x \quad (3)$$

$$Y(z) = (I z^p + \dots + Y_1 z + Y_0) \circ F_y \quad (4)$$

where  $X_i \in \mathbb{R}^{m \times n}$ ,  $Y_i \in \mathbb{R}^{n \times n}$  are numerical matrices containing the controller parameters,  $F_x, F_y$  are transfer function matrices containing desired fixed terms and  $\circ$  is the element-wise matrix multiplication. Fixed terms are terms that must be part of the final controller and are chosen based on a priori knowledge, such as integrators or resonant filters. This formulation offers a very flexible and effective framework where the controller structure and order can be defined rather freely. As the design takes place in the frequency-domain, discrete-time controllers can be designed using the frequency response of either a discrete- or continuous-time plant. It should also be noted that most controllers commonly used in power electronics can be easily expressed in this form, as shown in the following examples.

#### Example - PI controller with Lead/Lag compensators:

A very well-known structure that can be represented is a PI controller with filters. For example, a PI with two lead/lag compensators can be expressed as a third-order transfer function with fixed integrator:

$$\left( k_p + k_i \frac{1}{z-1} \right) \frac{z-b_1}{z-a_1} \frac{z-b_2}{z-a_2} = \frac{X_1 z^3 + X_2 z^2 + X_1 z + x_0}{(z^2 + Y_1 z + Y_0) \cdot (z-1)} = \frac{X(z)}{Y(z)} \quad (5)$$

**Example - Decentralized PI controller:** Assume a multi-variable system with three devices, where each device has a single input and a single output. To design a decentralized PI controller, the following structure can be chosen:

$$X(z) = \begin{bmatrix} X_1^{11} z + X_0^{11} & 0 & 0 \\ 0 & X_1^{22} z + X_0^{22} & 0 \\ 0 & 0 & X_1^{33} z + X_0^{33} \end{bmatrix}$$

$$Y(z) = \begin{bmatrix} 1 & 0 & 0 \\ 0 & 1 & 0 \\ 0 & 0 & 1 \end{bmatrix} \circ \begin{bmatrix} z-1 & 0 & 0 \\ 0 & z-1 & 0 \\ 0 & 0 & z-1 \end{bmatrix} \quad (6)$$

### C. Frequency-Domain Control Specifications

The desired control performance is defined as constraints on the norm of weighted sensitivity functions. This section will present some examples of how typical specifications can easily be transformed to frequency-domain constraints.

**Performance:** A classical performance criterion is to minimize the tracking error of the step response in the time-domain. From Parseval's theorem, this can be achieved in the frequency-domain by minimizing the following norm:

$$\min_{X,Y} \|W_t S\|_2, \quad W_t = \frac{1}{s} \mathbf{I} \quad (7)$$

Another typical performance specification is the desired bandwidth of the closed-loop system. One way to achieve a certain bandwidth is through loop shaping, where the goal is to design a controller such that the open loop transfer function  $L = GK$  is close to a desired open-loop transfer function  $L_d$ :

$$\min_{X,Y} \|L - L_d\|_2, \quad L_d = \frac{\omega_c}{s} \mathbf{I} \quad (8)$$

where  $\omega_c$  is the desired crossover frequency in rad/s.

If the system contains significant resonance modes, their influence on the closed-loop performance can be limited by

shaping the closed-loop sensitivity transfer functions. One possibility to achieve a certain closed-loop bandwidth and to limit the impact of an output disturbance on the tracking error is to minimize the following norm:

$$\min_{X,Y} \|W_1 S\|_\infty, \quad W_1 = \left( \frac{s\omega_{bw}}{s + \omega_{bw}} \right)^{-1} \mathbf{I} \quad (9)$$

where  $\omega_{bw}$  is the desired closed-loop bandwidth,  $S = (\mathbf{I} + GK)^{-1}$  is the sensitivity function and  $W_1$  is the performance weight. This choice of weight minimizes the tracking error at low frequencies, limits any peaks introduced by the resonances of the plant, and enforces a decoupling of the closed-loop system, which is an additional desired property.

The resonance modes of the plant generally appear in the closed-loop response  $T = GK(\mathbf{I} + GK)$ , which leads to oscillations in the time domain. An option to design a controller such that these oscillations are damped is by imposing a roll-off constraint on the closed-loop sensitivity:

$$\|W_2 T\|_\infty, \quad W_2 = \left( \alpha \frac{\omega_{bw}}{s + \omega_{bw}} \right)^{-1} \mathbf{I} \quad (10)$$

where  $\alpha > 1$  is a free parameter, and the shape of  $W_2$  is the inverse of a first-order low-pass filter. This constraint also improves the gain and phase margins, and limits the maximum overshoot in the time domain.

To limit large input action and to prevent fast input oscillations it is generally advisable to put a constraint on the input sensitivity  $U = K(\mathbf{I} + GK)$ , for example:

$$\|W_3 U\|_\infty, \quad W_3 = (\beta B)^{-1} \mathbf{I} \quad (11)$$

where  $\beta$  is a free parameter that limits the sensitivity of the inputs to an output disturbance, and  $B$  is a second-order discrete-time Butterworth low-pass filter. The cutoff frequency of  $B$  is another tuning parameter and should be chosen such that the sensitivity of the inputs towards high-frequency noise is low.

**Robustness:** If the system has different frequency responses in different operating points (e.g. due to changes in the grid topology), this can be represented by a multimodel uncertainty set, where the dynamics at each operating point are described by a separate model. Then, it is straightforward to design a controller that guarantees robust stability and performance for all the different models.

### D. Formulation of the Convex Optimization Problem

In order to compute the controller parameters, the robust control design problem can be rewritten as a convex optimization problem, which can be solved easily using standard optimization tools. A detailed overview of how to formulate and solve the convex problem is given in Appendix A.

## III. FREQUENCY-DOMAIN GRID MODELLING

It was described in Section II-A that the frequency-domain data of the plant is a required parameter for the control design, and that it can be obtained from a parametric (white-box) model or from time-domain measurements. In this paper, the

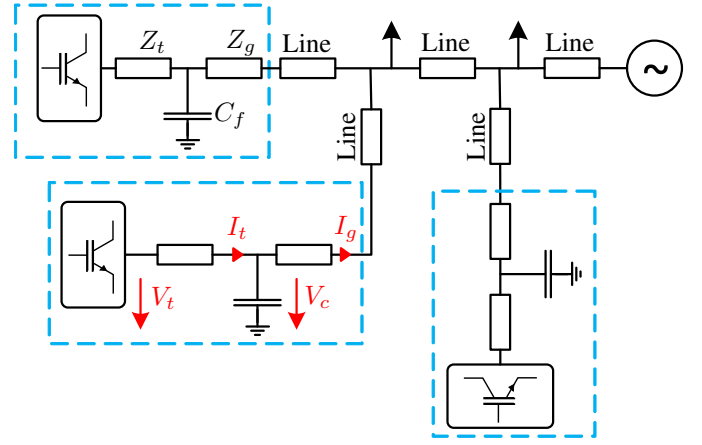


Fig. 2. One-line diagram of a distribution grid with multiple VSIs and constant current loads.

frequency response is computed from a parametric white-box model. This section presents a transfer function model that accurately describes the voltage and current dynamics in a grid with any number of inverters with LCL output filters, including the electromagnetic dynamics of the lines, output filters and coupling effects. It should be noted that the dynamics of the controllers have been treated in Section II, and are not part of the model. The model is formulated directly in the dq-frame, which is advantageous for the control design. The presented frequency-domain formulation offers the same modeling accuracy as a state-space small-signal model, but does not contain any internal state variables, which greatly reduces the model complexity.

For this paper, all three-phase voltages and currents are assumed to be balanced. VSIs are modeled using average models, and the dc-side dynamics are neglected. Figure 2 shows an example of a typical grid with multiple power electronic devices.

### A. Line Current Dynamics

For low-voltage grids, lines can be modeled as R-L elements. Furthermore, the line resistance and inductance matrix are assumed to be positive definite and circulant [28], which means symmetrical components can be used to study the system. With the assumption that all three-phase voltages and currents are balanced, only the positive sequence network needs to be considered. Considering the example in Fig. 2, the current flowing through a line from a bus  $i$  to a bus  $k$  can be formulated as follows:

$$(R_{ik} + j\omega_0 L_{ik})\underline{i}_{ik}(t) + L_{ik} \frac{d}{dt} \underline{i}_{ik}(t) = \underline{v}_i(t) - \underline{v}_k(t) \quad (12)$$

where  $\underline{v}_i(t) = v_{i,d}(t) + jv_{i,q}(t)$ ,  $\underline{i}_{ik}(t) = i_{ik,d}(t) + ji_{ik,q}(t)$  are the complex bus voltages and line current.  $\omega_0$  is the nominal grid frequency and  $R_{ik}, L_{ik}$  are scalars describing the positive sequence line resistance and inductance. Going to the frequency domain results in the following Laplace transfer function form:

$$(R_{ik} + j\omega_0 L_{ik})\underline{I}_{ik}(s) + sL_{ik}\underline{I}_{ik}(s) = \underline{V}_i(s) - \underline{V}_k(s) \quad (13)$$

where  $\underline{V}_i(s) = V_{i,d}(s) + jV_{i,q}(s)$ ,  $\underline{I}_{ik}(s) = I_{ik,d}(s) + jI_{ik,q}(s)$  are the Laplace transform of the voltages and currents. This can be rephrased as follows:

$$\underline{I}_{ik}(s) = \frac{sL_{ik} + R_{ik} - j\omega_0 L_{ik}}{(sL_{ik} + R_{ik})^2 + (\omega_0 L_{ik})^2} (\underline{V}_i(s) - \underline{V}_k(s)) \quad (14)$$

The argument ( $s$ ) is generally omitted for the rest of this paper. By separating the equation into its real and complex part, the matrix transfer function of the line current in the dq-frame can be formulated:

$$\begin{bmatrix} I_{ik,d} \\ I_{ik,q} \end{bmatrix} = \frac{1}{D} \begin{bmatrix} sL_{ik} + R_{ik} & \omega_0 L_{ik} \\ -\omega_0 L_{ik} & sL_{ik} + R_{ik} \end{bmatrix} \begin{bmatrix} V_{i,d} - V_{k,d} \\ V_{i,q} - V_{k,q} \end{bmatrix} \quad (15)$$

$$D = (sL_{ik} + R_{ik})^2 + (\omega_0 L_{ik})^2$$

It is assumed that each bus in the grid is either connected to a VSI with LCL output filter, or to a constant current load. Furthermore, the grid-side impedances  $Z_g$  of the LCL filters are lumped with the lines, and the voltage at a VSI bus is assumed to be the capacitor voltage  $V_c$ . Then, the following vectors are defined:

$$\underline{I}_{g,dq}^{\mathcal{I}} = [I_{g,d}^1, I_{g,q}^1, \dots, I_{g,d}^n, I_{g,q}^n]^T \quad (16)$$

$$\underline{V}_{c,dq}^{\mathcal{I}} = [V_{c,d}^1, V_{c,q}^1, \dots, V_{c,d}^n, V_{c,q}^n]^T \quad (17)$$

where  $n$  is the number of VSIs in the grid,  $\underline{I}_{g,dq}^{\mathcal{I}}$  is a vector with all VSI grid currents (named  $I_g$  in Fig. 2) and  $\underline{V}_{c,dq}^{\mathcal{I}}$  is a vector with all capacitor voltages of the LCL output filters (named  $V_c$  in Fig. 2).

Using Kirchhoff's Current Law and the transfer function from Eq. 15 the current-balance equations for every bus can be formulated:

$$\underbrace{\begin{bmatrix} Y_1(s) & Y_2(s) \\ Y_3(s) & Y_4(s) \end{bmatrix}}_{Y(s)} \begin{bmatrix} \underline{V}_{c,dq}^{\mathcal{I}} \\ \underline{V}_{dq}^{\mathcal{N}} \end{bmatrix} = \begin{bmatrix} \underline{I}_{g,dq}^{\mathcal{I}} \\ \underline{I}_{dq}^{\mathcal{L}} \end{bmatrix} \quad (18)$$

where  $\underline{V}_{dq}^{\mathcal{N}}$  is a vector with the voltages at the load buses, and  $\underline{I}_{dq}^{\mathcal{L}}$  is a vector with the load currents.  $Y_{1,\dots,4}$  are transfer function matrices according to Eq. 15. It is interesting to note that the frequency response evaluated at  $\omega_0$  of the matrix transfer function  $Y(j\omega_0)$  is equal to the nodal admittance matrix of the grid. However, to study stability it is necessary to consider the dynamic transfer function formulation  $Y(s)$ .

The load bus voltages can then be eliminated to achieve the following formulation of the VSI grid currents, with the load currents entering as a disturbance:

$$\begin{bmatrix} \underline{I}_{g,dq}^{\mathcal{I}} \end{bmatrix} = \underbrace{(Y_1 - Y_2 Y_4^{-1} Y_3)}_{Y_{\mathcal{I}}} \begin{bmatrix} \underline{V}_{c,dq}^{\mathcal{I}} \end{bmatrix} + \underbrace{Y_2 Y_4^{-1}}_{Y_d} \begin{bmatrix} \underline{I}_{dq}^{\mathcal{L}} \end{bmatrix} \quad (19)$$

This transfer function models the complete, coupled dynamics of the output currents of all VSIs in the grid depending on their capacitor voltages, with the load currents acting as disturbance. In [29], it is shown that  $Y_4$  is always invertible as long as all buses are connected, and all lines have non-zero resistance.

## B. LCL Filter Dynamics

To create a complete model, the dynamics of the LCL output filters need to be taken into account. Based on Fig. 2, the time-domain voltage and current dynamics of an LCL filter can be formulated as follows:

$$\dot{i}_t = C_f \frac{d}{dt} u_c + i_g \quad (20)$$

$$\underline{u}_t - \underline{u}_c = R_t \dot{i}_t + L_t \frac{d}{dt} i_t \quad (21)$$

where  $Z_t = R_t + j\omega_0 L_t$  is the inverter-side impedance of the filter.  $\underline{u}_t, \underline{u}_c$  are the complex terminal voltage and capacitor voltage, and  $\dot{i}_t, \dot{i}_c$  are the complex inverter-side and grid-side current of the VSI.

By inserting Eq. 20 into Eq. 21 and applying the Laplace transform the following transfer function can be obtained:

$$\begin{aligned} & (L_t C_f (-\omega_0^2 + 2j\omega_0 s + s^2) + R_t C_f (j\omega_0 + s) + 1) \underline{V}_c \\ & = \underline{V}_t - (R_t + j\omega_0 L_t + s) \underline{I}_g \end{aligned} \quad (22)$$

By separating the equation into its real and complex part the following transfer function matrix can be formulated:

$$\begin{bmatrix} V_{c,dq} \end{bmatrix} = \begin{bmatrix} G_{5,1} & -G_{5,2} \\ G_{5,2} & G_{5,1} \end{bmatrix}^{-1} G_6 \begin{bmatrix} V_{t,dq} \\ I_{g,dq} \end{bmatrix} \quad (23)$$

$$G_{5,1} = s^2 L_t C_f + s R_t C_f + (1 - L_t C_f \omega_0^2)$$

$$G_{5,2} = s^2 L_t C_f \omega_0 + R_t C_f \omega_0$$

$$G_6 = \begin{bmatrix} 1 & 0 & -(sL_t + R_t) & L_t \omega_0 \\ 0 & 1 & -L_t \omega_0 & -(sL_t + R_t) \end{bmatrix}$$

Furthermore, from Eq. 15 it can be written:

$$\begin{bmatrix} I_{t,dq} \end{bmatrix} = \begin{bmatrix} G_7 & -G_7 \end{bmatrix} \begin{bmatrix} V_{t,dq} \\ V_{c,dq} \end{bmatrix} \quad (24)$$

$$G_7 = \frac{1}{(sL_t + R_t)^2 + (\omega_0 L_t)^2} \begin{bmatrix} sL_t + R_t & \omega_0 L_t \\ -\omega_0 L_t & sL_t + R_t \end{bmatrix}$$

Now, the filter dynamics for all VSIs in the grid can be written in compact matrix form:

$$\begin{bmatrix} \underline{V}_{c,dq}^{\mathcal{I}} \end{bmatrix} = G^{V_t \rightarrow V_c} \begin{bmatrix} \underline{V}_{t,dq}^{\mathcal{I}} \end{bmatrix} + G^{I_g \rightarrow V_c} \begin{bmatrix} \underline{I}_{g,dq}^{\mathcal{I}} \end{bmatrix} \quad (25)$$

$$\begin{bmatrix} \underline{I}_{t,dq}^{\mathcal{I}} \end{bmatrix} = G^{V_t \rightarrow I_t} \begin{bmatrix} \underline{V}_{t,dq}^{\mathcal{I}} \end{bmatrix} + G^{V_c \rightarrow I_t} \begin{bmatrix} \underline{V}_{c,dq}^{\mathcal{I}} \end{bmatrix} \quad (26)$$

where  $G^{V_t \rightarrow V_c}, G^{I_g \rightarrow V_c}$  are matrix transfer functions according to Eq. 23, and  $G^{V_t \rightarrow I_t}, G^{V_c \rightarrow I_t}$  are matrix transfer functions according to Eq. 24.

## C. Complete Transfer Function Model

Based on the transfer functions derived above, a transfer function model of the complete system can be constructed. A block diagram of the model with the individual subsystems is shown in Fig. 3, where  $K$  is the current controller to be designed. From this block diagram, the matrix transfer function from the modulation voltages and load currents to the inverter currents can be computed:

$$\begin{bmatrix} \underline{I}_{t,dq}^{\mathcal{I}} \end{bmatrix} = G_{\text{complete}} \begin{bmatrix} \underline{V}_{t,dq}^{\mathcal{I}} \end{bmatrix} + G_d \begin{bmatrix} \underline{I}_{dq}^{\mathcal{L}} \end{bmatrix} \quad (27)$$

$$G_{\text{complete}} = G^{V_t \rightarrow I_t} + G^{V_c \rightarrow I_t} (\mathbf{I} - G^{I_g \rightarrow V_c} Y_{\mathcal{I}})^{-1} G^{V_t \rightarrow V_c}$$

$$G_d = G^{V_c \rightarrow I_t} G^{I_g \rightarrow V_c} (\mathbf{I} - G^{I_g \rightarrow V_c} Y_{\mathcal{I}})^{-1} Y_d$$

This frequency-domain model describes well the electro-magnetic dynamics of the complete grid, including the dynamics of the LCL output filters and coupling effects. It is also straightforward to extend in order to include the inverter dynamics in more details, or to reshape in order to design a voltage controller. Another possible extension would be the inclusion of more complex load models.

#### IV. APPLICATION EXAMPLE: DESIGN OF DECENTRALIZED CONTROLLER FOR VSIS IN A DISTRIBUTION GRID

In this section, the presented control design method is applied to design robust current controllers for multiple VSIs in a 50 Hz/400 V rural distribution grid based on a real case. The distribution grid with four inverter-interfaced PV generation units is shown in Fig. 4a) (for simplicity, the loads and the dc-side dynamics are neglected). As commonly occurring in these grid configurations, the VSI buses suffer from overvoltage problems during high PV production. Moreover, since the lines are mostly resistive, reactive power injection has almost no effect on the voltage level. To resolve this issue, a Line Voltage Regulator (LVR) is added to the grid, which consists of a tap-changing transformer that is activated whenever an overvoltage is detected. However, the LVR also increases the inductance of the line, which has a significant impact on the electromagnetic dynamics of the grid, as shown below.

The goal is to design in a single step the current controllers for all four VSIs such that stability is guaranteed, and certain performance specifications are satisfied for both grid configurations (without and with the LVR). The LVR is modelled as an R-L element using the simplified equivalent circuit transformer model. Figure 4b) shows a single-line diagram of the output filter and current controller structure of an individual VSI, where  $K_i$  is the  $2 \times 2$  transfer function controller of VSI  $i$  to be designed. A second-order generalized integrator based PLL (SOGI-PLL) is used due to its favorable robustness properties [30].

##### A. Grid Model

Two transfer function models for the grid without and with the LVR are constructed according to Equation 27. The grid-side impedances  $Z_g$  of the filters and the impedance of the LVR are lumped with the lines. To visualize the effect of the LVR on the frequency response of the system, the maximum singular value plots of  $G_{\text{complete}}$  for both grid configurations are shown in Fig. 5. The singular value plot is an extension of the Bode magnitude plot for multivariable systems, and is a very useful tool for robustness analysis [31].

The expected resonance peaks of the LCL output filters can be seen around 1400 Hz. However, the model without LVR also exhibits additional resonance peaks at 1200 Hz that stem from the coupling of the LCL filters, and would not be represented in a classical single-inverter model. Furthermore, with the inclusion of the LVR the frequency of the coupling resonance decreases to 1000 Hz and dominates the dynamic response, which further accentuates the importance of using a complete grid model.

##### B. Control Design

A decentralized, multivariable 4th-order controller with a sampling frequency of 10 kHz is designed, where every VSI has access only to its local current measurements. The controllers of the 4 VSIs in Fig. 4 can be compounded as a single block-diagonal transfer function matrix according to the multivariable plant model from Eq. 27:

$$\begin{aligned}
 K &= \begin{bmatrix} K_1^{1,1} & K_1^{1,2} & & & & \\ K_1^{2,1} & K_1^{2,2} & & & & \\ & & \ddots & & & \\ & & & K_4^{1,1} & K_4^{1,2} & \\ & & & K_4^{2,1} & K_4^{2,2} & \\ & & & & & \ddots & \\ & & & & & & X_4^{1,1} & X_4^{1,2} \\ & & & & & & X_4^{2,1} & X_4^{2,2} \\ & & & & & & & \ddots & \\ & & & & & & & & Y_4^{1,1} & \\ & & & & & & & & & Y_4^{2,2} \end{bmatrix} = XY^{-1} \\
 X &= \begin{bmatrix} X_1^{1,1} & X_1^{1,2} & & & & \\ X_1^{2,1} & X_1^{2,2} & & & & \\ & & \ddots & & & \\ & & & X_4^{1,1} & X_4^{1,2} & \\ & & & X_4^{2,1} & X_4^{2,2} & \\ & & & & & \ddots & \\ & & & & & & Y_4^{1,1} & \\ & & & & & & & Y_4^{2,2} \end{bmatrix} \\
 Y &= \begin{bmatrix} Y_1^{1,1} & & & & & \\ & Y_1^{2,2} & & & & \\ & & \ddots & & & \\ & & & Y_4^{1,1} & & \\ & & & & Y_4^{2,2} & \end{bmatrix} \circ (z-1)\mathbf{I} \\
 X_k^{i,j} &= X_{k,4}^{i,j}z^4 + X_{k,3}^{i,j}z^3 + X_{k,2}^{i,j}z^2 + X_{k,1}^{i,j}z + X_{k,0}^{i,j} \\
 Y_k^{i,j} &= z^4 + Y_{k,3}^{i,j}z^3 + Y_{k,2}^{i,j}z^2 + Y_{k,1}^{i,j}z + Y_{k,0}^{i,j} \quad (28)
 \end{aligned}$$

where  $X$  has a block-diagonal and  $Y$  has a diagonal structure. The final  $2 \times 2$  controller of each individual VSI contains 28 tunable parameters, which allows for many degrees of freedom during the design, but would be very difficult to tune manually.

The controller should satisfy the following performance specifications for both grid configurations (without and with the LVR):

- 1) Closed-loop bandwidth of at least 500 Hz
- 2) Small overshoot
- 3) Robustness towards modeling errors
- 4) Good decoupling of currents in d and q axis

As described in Section II-C, the first specification can be achieved through the following objective function:

$$\min_{X,Y} (\max(\|W_1 S_1\|_\infty, \|W_1 S_2\|_\infty)), \quad W_1 = \left( \frac{s \omega_{bw}}{s + \omega_{bw}} \right)^{-1} \mathbf{I} \quad (29)$$

where  $\omega_{bw} = 2\pi \cdot 500$  is the desired bandwidth and  $S_i = (I + G_i K)^{-1}$  are the sensitivity transfer functions for the two plants (without and with the LVR).

Similarly, the second and third specifications are satisfied by placing constraints on the two closed-loop sensitivity functions  $T_i = G_i K (I + G_i K)^{-1}$ :

$$\|W_2 T_1\|_\infty < 1, \quad \|W_2 T_2\|_\infty < 1; \quad W_2 = \left( 1.1 \frac{\omega_{bw}}{s + \omega_{bw}} \right)^{-1} \mathbf{I} \quad (30)$$



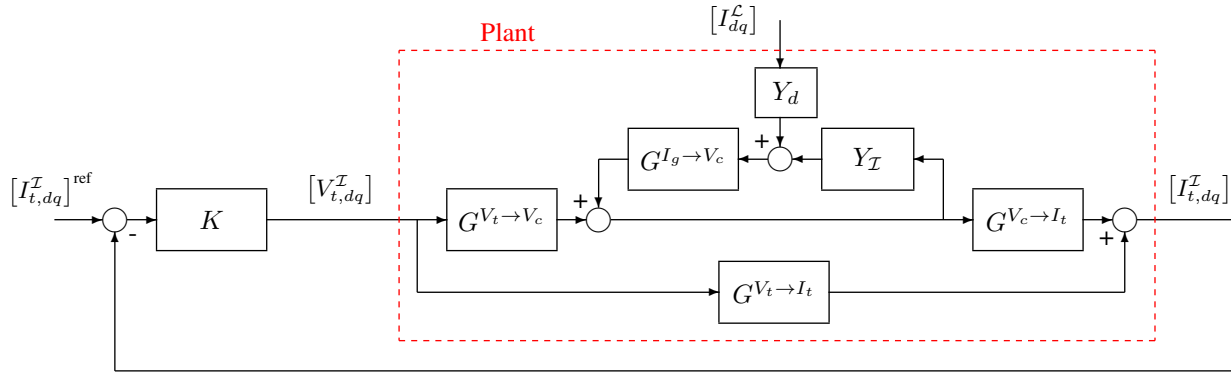


Fig. 3. Block diagram of the complete closed-loop model.

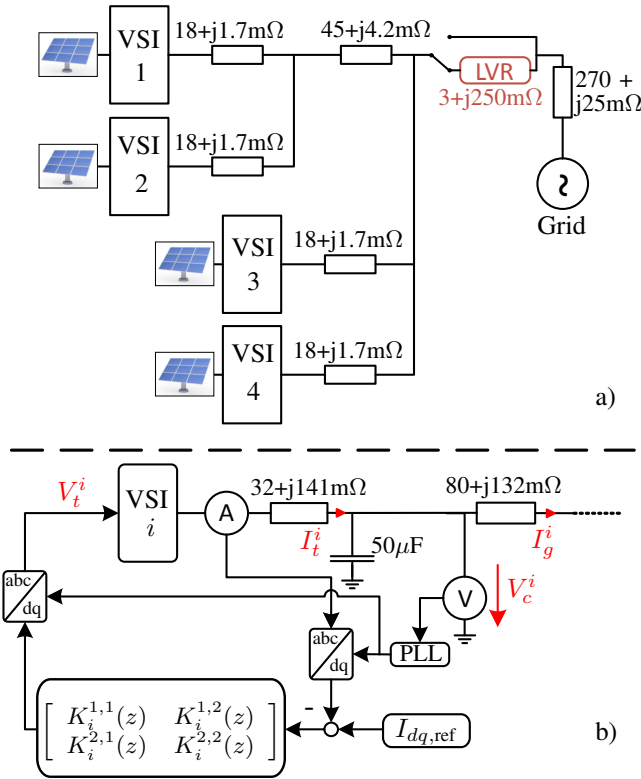


Fig. 4. Electrical one-line diagrams: a) a rural distribution grid with 4 identical VSIs and a Line Voltage Regulator (LVR), b) the output filter configuration and controller block diagram of the VSIs.

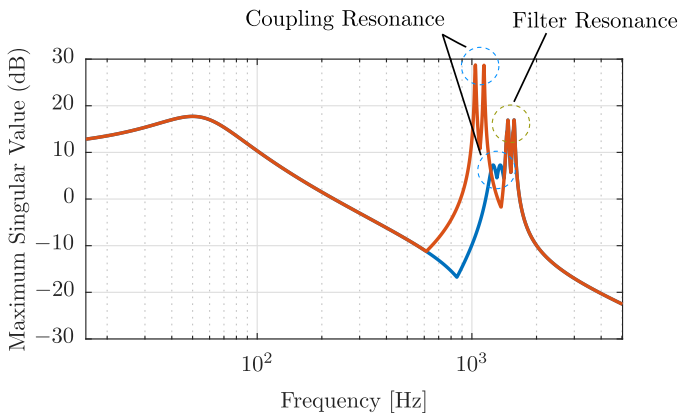


Fig. 5. Maximum singular value plots of the grid model. The model without the LVR is in blue, and with the LVR in red.

Finally, a constraint is placed on the input sensitivities  $U_i = K(I + G_i K)^{-1}$ :

$$\|W_3 U_1\|_\infty < 1, \|W_3 U_2\|_\infty < 1; W_3 = (5.5B)^{-1} \mathbf{I} \quad (31)$$

where  $B$  is a second-order discrete-time Butterworth low-pass filter with a cutoff frequency of 2500 Hz.

These constraints are combined to formulate the following robust control design problem, where  $\gamma \in \mathbb{R}$  is an auxiliary scalar variable:

$$\begin{aligned} & \min_{X,Y} \gamma \\ & \text{subject to:} \\ & \|W_1 S_1\|_\infty < \gamma, \|W_1 S_2\|_\infty < \gamma \\ & \|W_2 T_1\|_\infty < 1, \|W_2 T_2\|_\infty < 1 \\ & \|W_3 U_1\|_\infty < 1, \|W_3 U_2\|_\infty < 1 \end{aligned} \quad (32)$$

Using the method from [27] the problem is reformulated as a convex optimization problem (see Appendix A-D for more details). The optimization is solved in Matlab using Yalmip [32] and Mosek [33]. The algorithm converges within less than 30 minutes on a standard laptop computer for our simple implementation.

The singular value plots of the controller as well as the achieved sensitivities are shown in Fig. 6. In Fig. 6a) it can be seen that the frequency response of the controller cancels the resonance peaks of the plant as expected, and is also robust towards plant uncertainties. Specifically, even if the resonance frequencies in the real grid are different from the model, they are still sufficiently attenuated. In the closed-loop response in Fig. 6b) it can be seen that the filter and coupling resonances are sufficiently damped, and that the desired bandwidth is achieved. Furthermore, the constraints on the closed-loop and input sensitivity are satisfied.

### C. Simulation Results

To verify the controller performance, the example grid from Fig. 4 is implemented in MATLAB/Simulink using the SimPowerSystems toolbox. An averaged model is used for the VSIs, and the switching and dc-side dynamics are neglected. The step response of the inverter current of VSI 1 without and with the LVR is shown in Fig. 7. It can be seen that the transients are smooth and there is no ringing. The top of the figure shows a zoomed-in view of the step responses

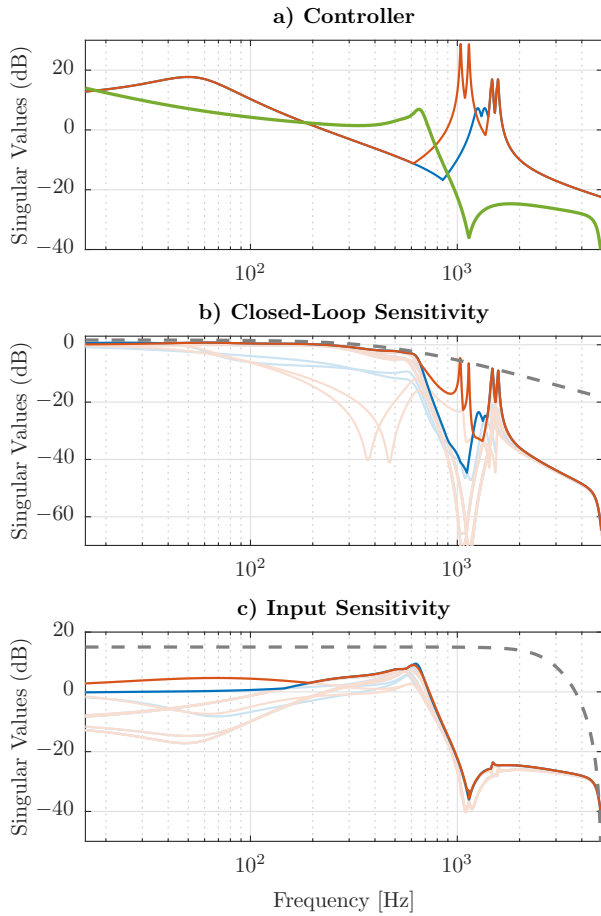


Fig. 6. Frequency response plots: a) Maximum singular values of the designed controller (in green) and the plant without and with the LVR (in blue and red). b) Singular value plot of the closed-loop sensitivities and c) singular value plot of the input sensitivities without and with the LVR (in blue and red). The solid lines denote the maximum singular values, and the dashed lines indicate the constraints

of  $I_{t,d}^1$  and  $I_{t,q}^1$  without the LVR, with the 10-90 % rise-times being 1.2 ms. With the LVR, the rise times are slower at 4.5 ms and 4.6 ms. These values correspond well with the minimum desired closed-loop bandwidth of 500 Hz. The maximum overshoot is 6.7 %, and the decoupling of the d-q axes is excellent. The step responses of the VSIs 2, 3 and 4 exhibit almost equal performance, but are not shown due to space constraints.

#### D. Plug-and-Play Design

The control design method can also be used for plug-and-play design, where the goal is to design a current controller for a new VSI that is added to an existing grid, without retuning the current controllers of the other VSIs.

Consider again the example presented in the previous section, and let  $K_{\text{fixed}}$  be the current controller designed for VSIs 1 through 4. The goal is to design a current controller for a new VSI 5 connected at bus 3 in a decentralized fashion and without changing  $K_{\text{fixed}}$ . Again, as described in Section III, two transfer function models of the grid without and with the

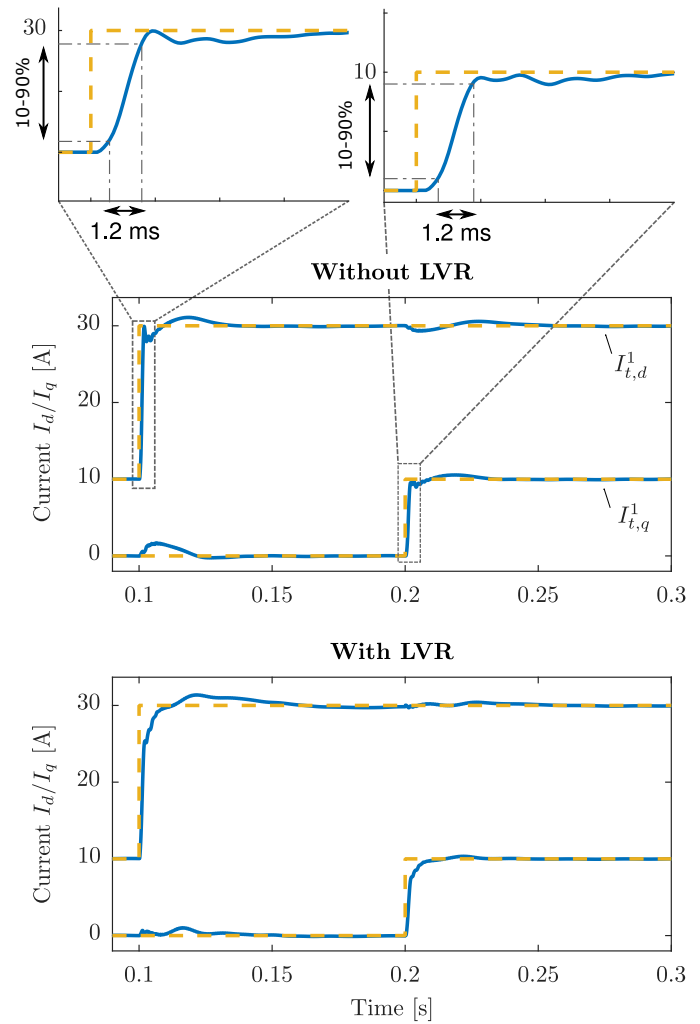


Fig. 7. Inverter current step response of VSI 1 without and with the LVR. The dashed line shows the current reference.

LVR are constructed. Then, the existing controller  $K_{\text{fixed}}$  is used to close the feedback loops for VSIs 1 through 4 (see Fig. 9). This allows to form a new plant with only two inputs and two outputs, where the inputs are the modulation voltage and the outputs are the inverter current of VSI 5. The same performance specifications on the rise-time and overshoot as in the previous section are used, and a controller is designed. The grid is again simulated in Simulink, and the step response of the inverter current of VSI 5 without and with the LVR is shown in Fig. 10.

The 10-90 % rise-times of  $I_{t,d}^5, I_{t,q}^5$  are 1.4 ms and 1.1 ms without the LVR, and 5.1 ms and 1.5 ms with the LVR, which again satisfies the specifications. The overshoot is larger than for the centrally designed controller, but is still limited to 10 %, and the decoupling is good.

## V. EXPERIMENTAL RESULTS

To validate the simulation results obtained in the previous section, the converter controllers are implemented on an experimental setup suited for power hardware in the loop (PHIL) testing, and their performance is assessed.



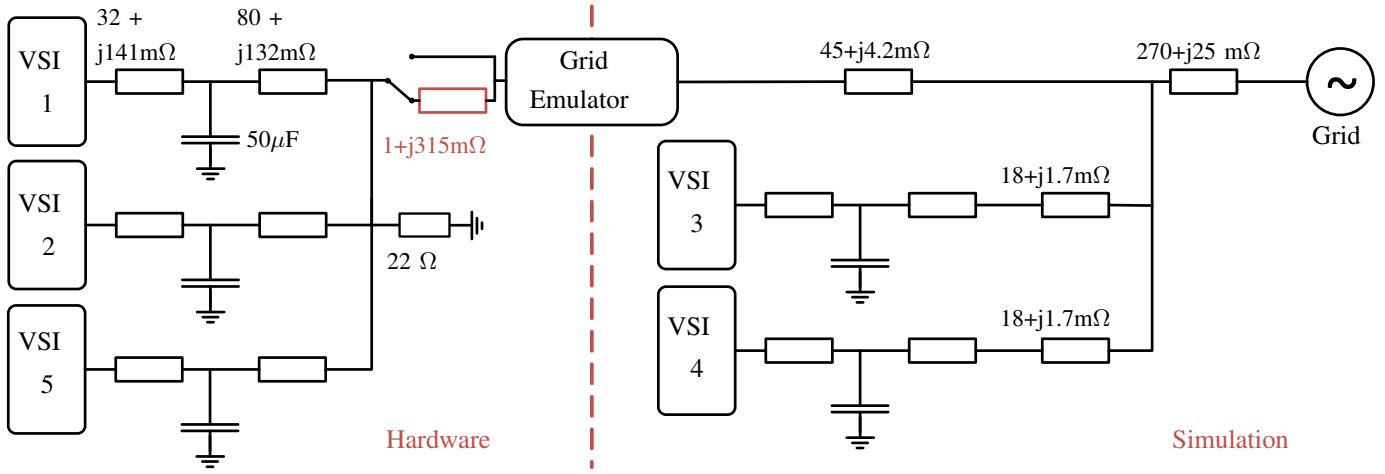


Fig. 8. One-line diagram of the PHIL setup. The output filter impedances are identical for all VSIs.

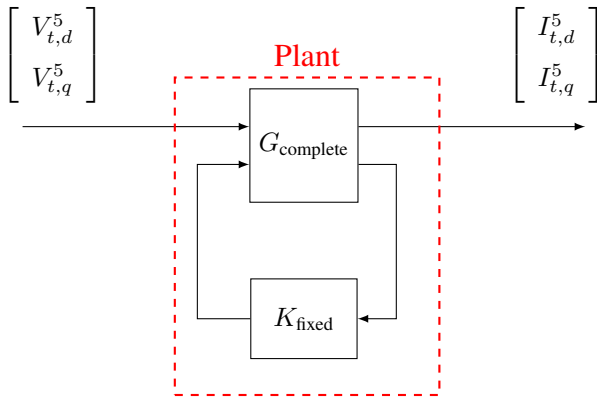


Fig. 9. Block diagram of the model used for plug&play-design.

The grid layout of the PHIL experiments is shown in Fig. 8. The grid bus and two VSIs are modeled in real-time simulation, while three VSIs and the LVR are real devices. The interface between the simulation and hardware side is provided by a grid emulator, which is described below. The setup also exhibits several differences compared to the simulation example. The hardware side does not contain the line impedances, and the position of the LVR has been moved such that it can be included on the hardware side. Additionally, a resistive  $22 \Omega$  load is added on the hardware side. For the PHIL experiment, the LVR is represented by an inductor with  $R_{LVR} = 1 \text{ m}\Omega$  and  $L_{LVR} = 1000 \mu\text{H}$ , with the change in voltage level being provided by the grid emulator.

The grid emulator is a 200 kW high bandwidth grid emulator (EGSTON-COMPISO). The three 2-level inverters are custom-designed prototypes with a rating of 60 kVA at 400 V ac (line-to-line RMS) and 700 V dc. They are identical in construction and are based on Semikron integrated IGBT modules. The converter terminals include an LCL filter on the ac side, and a dc bus capacitor with a capacitance of 4 mF. They are isolated from the grid though a decoupling transformer, the impedance of which is included in the grid impedance of the filter. The control of the converters is implemented entirely in

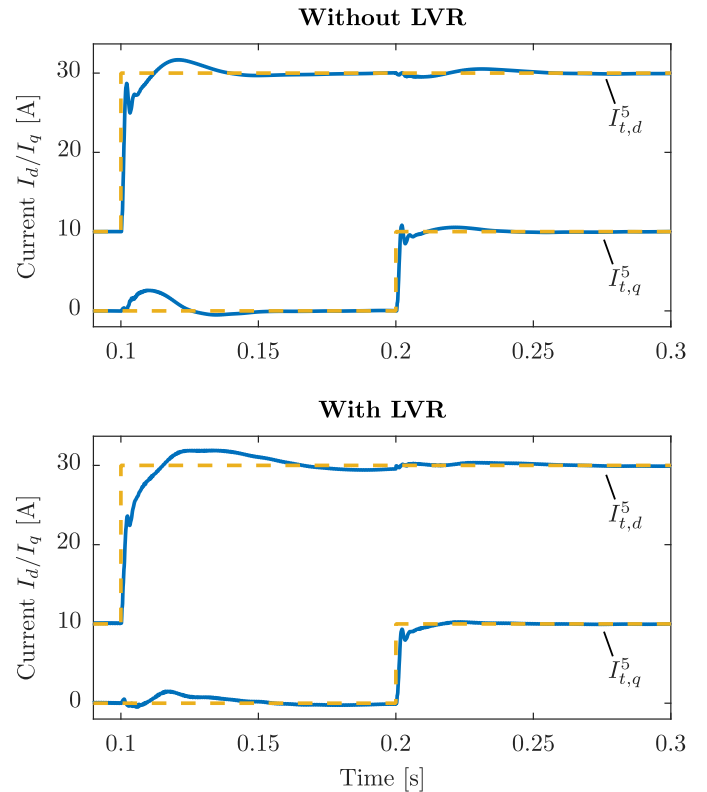


Fig. 10. Inverter current step response of the plug-and-play controller of VSI 5 without the LVR. The dashed line shows the current reference.

the OPAL-RT platform where a custom programmed FPGA dedicated to sampling and conditioning of the measurements and to the generation of the gate signals is also included. The inverters are connected to the same busbars both on the dc and ac side. Pictures of the experimental setup are shown in Fig. 11. Additionally, during the experiments, strong 5th and 7th harmonics were observed due to the switching dead-time of the VSIs. A harmonic compensation scheme based on multiple synchronous reference frames was added in order to reduce their effect [34].

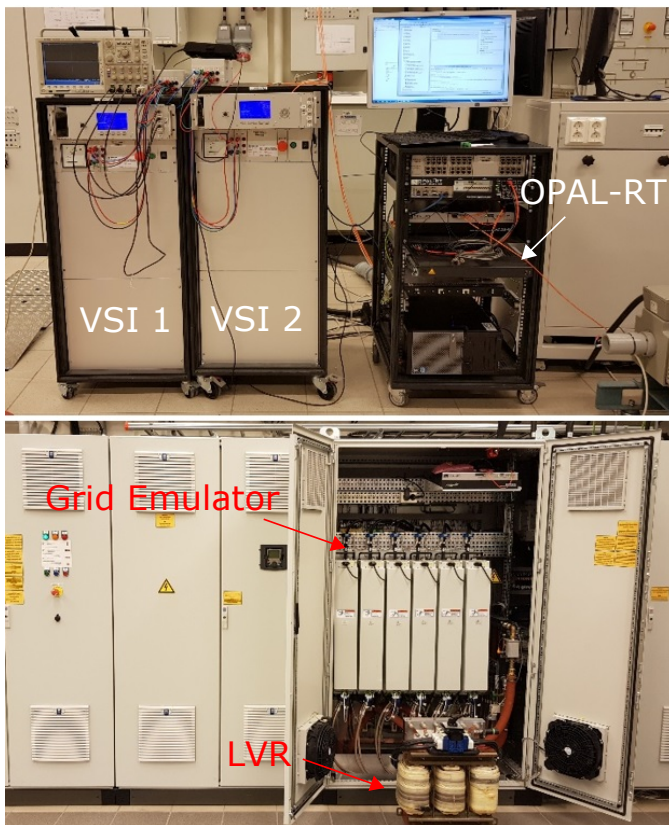


Fig. 11. Photos of the experimental setup. The top picture shows two of the VSIs used in the experiment as well as the OPAL-RT interface. The bottom picture shows the grid emulator and the inductance used to emulate the LVR.

### A. PHIL Results

It should be emphasized that the current controllers for the PHIL experiments were designed based on the nominal model of the grid in Fig. 4, which is quite different from the experimental setup. This conveniently illustrates the robustness of the designed controllers towards changes in the line impedances and grid layout.

The step response of the inverter current of VSI 1 without and with the LVR is shown in Fig. 12. Similarly, the inverter current step response of VSI 5 with the plug-and-play controller is shown in Figs. 13. It can be seen that the designed current controllers are able to guarantee the stability for both grid configurations in a PHIL setting. The obtained transient performance is very close to the simulation results. The difference in rise-time and overshoot are almost purely due to the harmonic oscillations present in the grid. It can also be seen that the harmonic oscillations are temporarily increased after the steps, which is due to the transient response of the harmonic compensation scheme.

Finally, the three-phase voltage and current measurements of VSI 1 during the step of  $I_{t,d}^1$  without and with the LVR are shown in Fig. 14. The obtained voltage waveform is clean, and only some minor high-frequency harmonic distortion is visible on the current.

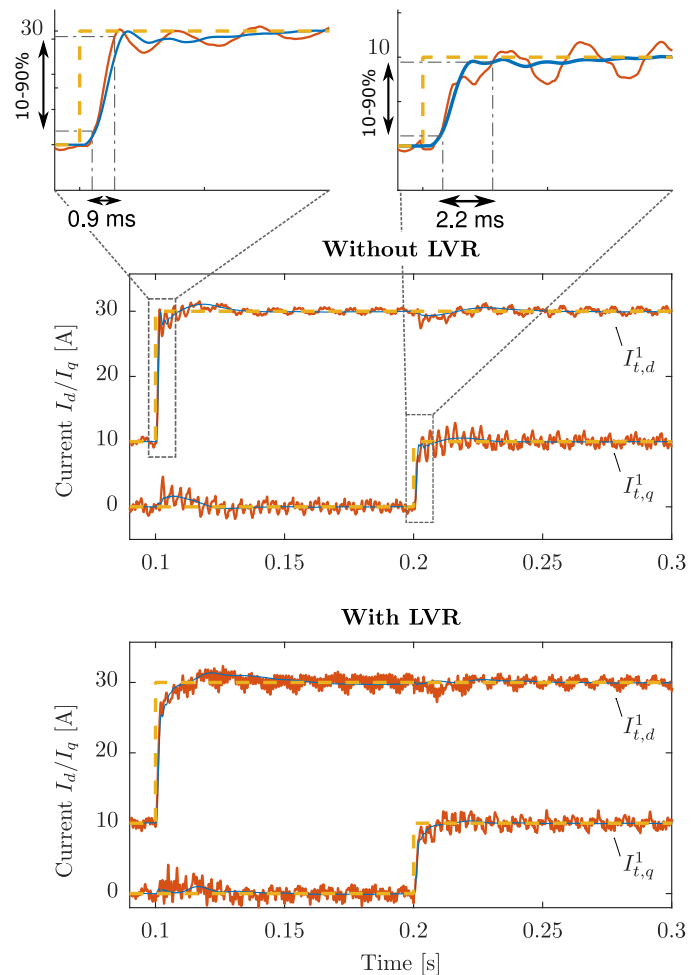


Fig. 12. Inverter current step response of VSI 1 without and with the LVR. The PHIL results are in red, simulation results are in blue, the dashed line shows the current reference.

## VI. CONCLUSION

A novel controller synthesis method for the current control design of multiple VSIs has been presented. Furthermore, a frequency-domain model was constructed that accurately models line, output filter and coupling dynamics. It was then shown how the control design method and model can be used to design higher-order, robust current controllers for multiple VSIs in a single step. Robust stability and performance are guaranteed a priori, and no iterative tuning is necessary. The effectiveness of the designed controllers in addressing the instability problems of power-electronics-based grids has been demonstrated in a realistic scenario through simulation as well as through experimental results on a PHIL setup. While in this paper a parametric model was used, the control design method also supports a fully data-driven approach, where the frequency response is calculated directly from measurement data. This very promising avenue will be explored in future works.

## REFERENCES

- [1] Ł. H. Kocewiak, J. Hjerrild, and C. L. Bak, "Wind turbine converter control interaction with complex wind farm systems," *IET Renewable Power Generation*, vol. 7, no. 4, pp. 380–389, 2013.

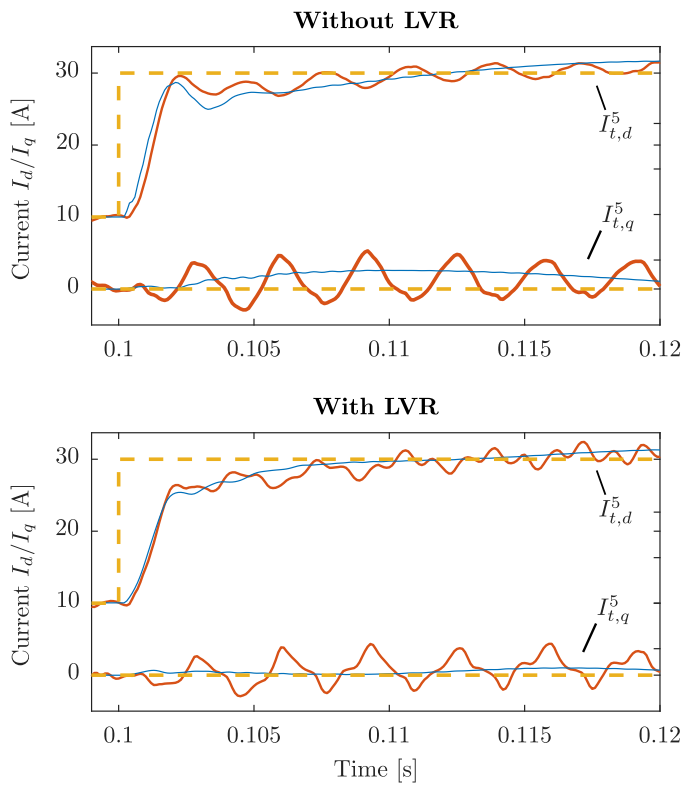


Fig. 13. Inverter current step response of the plug-and-play controller of VSI 5 without and with the LVR. The PHIL results are in red, simulation results are in blue, the dashed line shows the current reference.

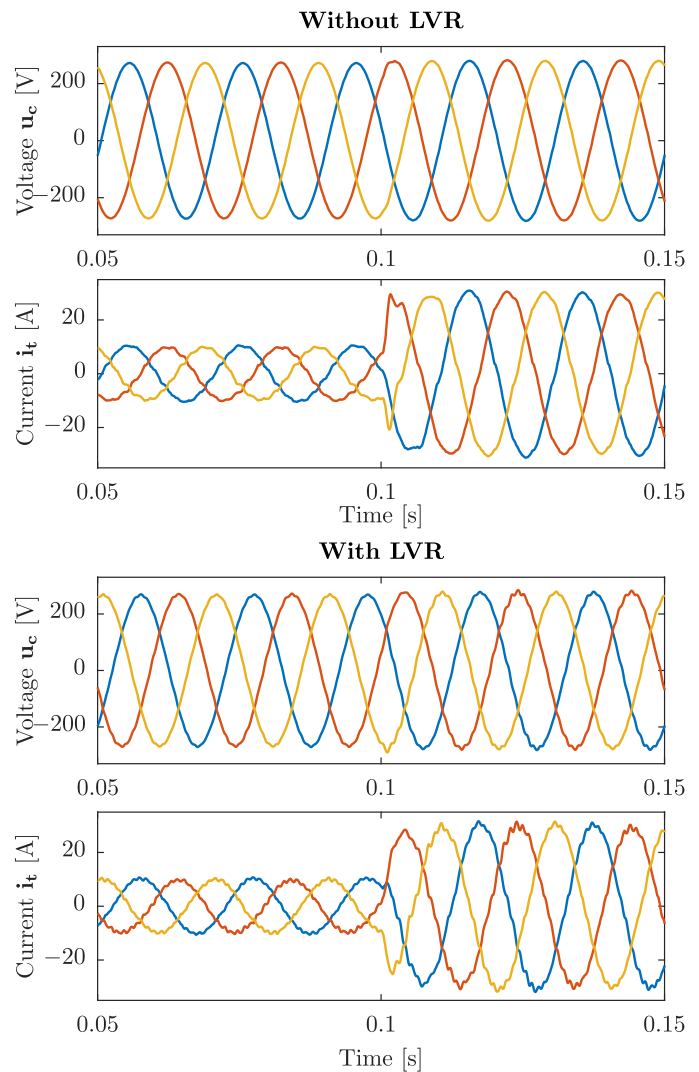


Fig. 14. Three-phase voltage and current of VSI 1 without and with the LVR during the step of  $I_{t,d}^1$ .

[2] X. Wang, F. Blaabjerg, Z. Chen, and W. Wu, "Resonance analysis in parallel voltage-controlled distributed generation inverters," in *Applied Power Electronics Conference and Exposition (APEC), 2013 Twenty-Eighth Annual IEEE*. IEEE, 2013, pp. 2977–2983.

[3] F. Wang, J. L. Duarte, M. A. Hendrix, and P. F. Ribeiro, "Modeling and analysis of grid harmonic distortion impact of aggregated DG inverters," *IEEE Transactions on Power Electronics*, vol. 26, no. 3, pp. 786–797, 2011.

[4] R. Turner, S. Walton, and R. Duke, "Stability and bandwidth implications of digitally controlled grid-connected parallel inverters," *IEEE Transactions on Industrial Electronics*, vol. 57, no. 11, pp. 3685–3694, 2010.

[5] J. He, Y. W. Li, D. Bosnjak, and B. Harris, "Investigation and active damping of multiple resonances in a parallel-inverter-based microgrid," *IEEE Transactions on Power Electronics*, vol. 28, no. 1, pp. 234–246, 2013.

[6] C. C. Gomes, A. F. Cupertino, and H. A. Pereira, "Damping techniques for grid-connected voltage source converters based on LCL filter: An overview," *Renewable and Sustainable Energy Reviews*, vol. 81, pp. 116–135, 2018.

[7] J. L. Agorreta, M. Borrega, J. López, and L. Marroyo, "Modeling and control of  $N$ -paralleled grid-connected inverters with LCL filter coupled due to grid impedance in PV plants," *IEEE Transactions on Power Electronics*, vol. 26, no. 3, pp. 770–785, 2011.

[8] M. Borrega, L. Marroyo, R. Gonzalez, J. Balda, and J. L. Agorreta, "Modeling and control of a master-slave PV inverter with  $N$ -paralleled inverters and three-phase three-limb inductors," *IEEE Transactions on Power Electronics*, vol. 28, no. 6, pp. 2842–2855, 2013.

[9] N. Pogaku, M. Prodanovic, and T. C. Green, "Modeling, analysis and testing of autonomous operation of an inverter-based microgrid," *IEEE Transactions on Power Electronics*, vol. 22, no. 2, pp. 613–625, 2007.

[10] Y. Wang, X. Wang, F. Blaabjerg, and Z. Chen, "Harmonic instability assessment using state-space modeling and participation analysis in inverter-fed power systems," *IEEE Transactions on Industrial Electronics*, vol. 64, no. 1, pp. 806–816, 2017.

[11] N. Bottrell, M. Prodanovic, and T. C. Green, "Dynamic stability of a microgrid with an active load," *IEEE Transactions on Power Electronics*, vol. 28, no. 11, pp. 5107–5119, 2013.

[12] B. Wen, D. Dong, D. Boroyevich, R. Burgos, P. Mattavelli, and Z. Shen, "Impedance-based analysis of grid-synchronization stability for three-phase paralleled converters," *IEEE Transactions on Power Electronics*, vol. 31, no. 1, pp. 26–38, 2016.

[13] X. Wang, F. Blaabjerg, and W. Wu, "Modeling and analysis of harmonic stability in an AC power-electronics-based power system," *IEEE Transactions on Power Electronics*, vol. 29, no. 12, pp. 6421–6432, 2014.

[14] M. Lu, X. Wang, F. Blaabjerg, and P. C. Loh, "An analysis method for harmonic resonance and stability of multi-paralleled LCL-filtered inverters," in *Power Electronics for Distributed Generation Systems (PEDG), 2015 IEEE 6th International Symposium on*. IEEE, 2015, pp. 1–6.

[15] M. Lu, X. Wang, P. C. Loh, and F. Blaabjerg, "Resonance interaction of multiparallel grid-connected inverters with LCL filter," *IEEE Transactions on Power Electronics*, vol. 32, no. 2, pp. 894–899, 2017.

[16] S. Yang, Q. Lei, F. Z. Peng, and Z. Qian, "A robust control scheme for grid-connected voltage-source inverters," *IEEE Transactions on Industrial Electronics*, vol. 58, no. 1, pp. 202–212, 2011.

[17] T. Hornik and Q.-C. Zhong, "A current-control strategy for voltage-source inverters in microgrids based on  $H_\infty$  and repetitive control," *IEEE Transactions on Power Electronics*, vol. 26, no. 3, pp. 943–952, 2011.

[18] G. Weiss, Q.-C. Zhong, T. C. Green, and J. Liang, " $H_\infty$  repetitive control of DC-AC converters in microgrids," *IEEE Transactions on Power Electronics*, vol. 19, no. 1, pp. 219–230, 2004.

[19] A. Kahrobaian and Y. A.-R. I. Mohamed, "Robust single-loop di-

- rect current control of LCL-filtered converter-based DG units in grid-connected and autonomous microgrid modes,” *IEEE Transactions on Power Electronics*, vol. 29, no. 10, pp. 5605–5619, 2014.
- [20] M. S. Sadabadi, A. Haddadi, H. Karimi, and A. Karimi, “A robust active damping control strategy for an LCL-based grid-connected DG unit,” *IEEE Transactions on Industrial Electronics*, 2017.
- [21] L. Maccari, J. Massing, L. Schuch, C. Rech, H. Pinheiro, V. Montagner, and R. Oliveira, “Robust  $\mathcal{H}_\infty$  control for grid connected PWM inverters with LCL filters,” in *Industry Applications (INDUSCON), 2012 10th IEEE/IAS International Conference on*. IEEE, 2012, pp. 1–6.
- [22] L. A. Maccari, J. R. Massing, L. Schuch, C. Rech, H. Pinheiro, R. C. Oliveira, and V. F. Montagner, “LMI-based control for grid-connected converters with LCL filters under uncertain parameters,” *IEEE Transactions on Power Electronics*, vol. 29, no. 7, pp. 3776–3785, 2014.
- [23] A. Egea-Alvarez, S. Fekriasl, F. Hassan, and O. Gomis-Bellmunt, “Advanced vector control for voltage source converters connected to weak grids,” *IEEE Transactions on Power Systems*, vol. 30, no. 6, pp. 3072–3081, 2015.
- [24] B. Bahrani and A. Rufer, “Optimization-based voltage support in traction networks using active line-side converters,” *IEEE Transactions on Power Electronics*, vol. 28, no. 2, pp. 673–685, 2013.
- [25] B. Bahrani, A. Karimi, B. Rey, and A. Rufer, “Decoupled dq-current control of grid-tied voltage source converters using nonparametric models,” *IEEE Transactions on Industrial Electronics*, vol. 60, no. 4, pp. 1356–1366, 2013.
- [26] B. Bahrani, M. Vasiladiotis, and A. Rufer, “High-order vector control of grid-connected voltage-source converters with LCL-filters,” *IEEE Transactions on Industrial Electronics*, vol. 61, no. 6, pp. 2767–2775, 2014.
- [27] A. Karimi and C. Kammer, “A data-driven approach to robust control of multivariable systems by convex optimization,” *Automatica*, vol. 85, pp. 227–233, 2017.
- [28] C. R. Paul, *Analysis of multiconductor transmission lines*. John Wiley & Sons, 2008.
- [29] A. M. Kettner and M. Paolone, “On the properties of the power systems nodal admittance matrix,” *arXiv preprint arXiv:1702.07235*, 2017.
- [30] P. Cossutta, S. Raffo, A. Cao, F. Ditaranto, M. P. Aguirre, and M. I. Valla, “High speed single phase SOGI-PLL with high resolution implementation on an FPGA,” in *Industrial Electronics (ISIE), 2015 IEEE 24th International Symposium on*. IEEE, 2015, pp. 1004–1009.
- [31] S. Skogestad and I. Postlethwaite, *Multivariable feedback control: analysis and design*. Wiley New York, 2007, vol. 2.
- [32] J. Löfberg, “YALMIP: A toolbox for modeling and optimization in MATLAB,” in *CACSD Conference*, <http://control.ee.ethz.ch/joloef/yalmip.php>, 2004.
- [33] MOSEK ApS, *The MOSEK optimization toolbox for MATLAB manual. Version 7.1*, 2015. [Online]. Available: <http://docs.mosek.com/7.1/toolbox/index.html>
- [34] P. Mattavelli, “A closed-loop selective harmonic compensation for active filters,” *IEEE Transactions on Industry Applications*, vol. 37, no. 1, pp. 81–89, 2001.